Scattering-angle dependence of doubly differential cross sections for fragmentation of H_{2} by proton impact

K. N. Egodapitiya, S. Sharma, A. C. Laforge, and M. Schulz

Phys. Rev. A **83**, 012709 — Published 26 January 2011

DOI: 10.1103/PhysRevA.83.012709

Scattering Angle Dependence of Double Differential Cross Sections for Fragmentation of H_2 by Proton Impact

K.N. Egodapitiya, S. Sharma, A.C. Laforge*, and M. Schulz

Dept. of Physics and LAMOR, Missouri University of Science & Technology, Rolla, MO 65409

We have measured double differential cross sections (DDCS) for proton fragment formation for fixed projectile energy losses as a function of projectile scattering angle in 75 keV p + H_2 collisions. An oscillating pattern was observed in the angular dependence of the DDCS with a frequency about twice as large as what we found earlier for non-dissociative ionization. Possible origins for this frequency doubling are discussed.

PACS no's: 34.50.Bw, 34.50.Fa, 34.50.Gb

* Present address: *Max-Planck-Institut für Kernphysik,Saupfercheckweg 1, 69117 Heidelberg, Germany*

Introduction

Collisions of charged particles with molecular hydrogen have been studied extensively over the last decade because H_2 represents the simplest target with multiple scattering centers [e.g. 1-14]. This property can give rise to various manifestations of quantum-mechanical interference in differential cross sections for ionization, electron capture, or other scattering processes. Already 50 years ago Tuan and Gerjuoy [15] presented a theoretical analysis of interference in the scattered projectile wave due to indistinguishable diffraction of the projectile from the two atomic centers in the molecule. But it was only more than 30 years later that interference effects were first reported in measured capture and ionization cross sections as a function of the molecular orientation [16].

The interest in molecular interference effects significantly intensified when they were observed in measured double differential cross sections as a function of the energy of electrons ejected from H_2 by highly charged ion impact [e.g. 1-3]. Here, the data were interpreted as interference in the ejected electron wave due to indistinguishable emission from the two atomic centers. However, the reported structures were not very pronounced; only after normalizing the data to calculations for atomic hydrogen an oscillation was observed. Significantly more pronounced interference structures were found in capture cross sections as a function of the molecular orientation in $He^{2+} + H_2$ collisions [10] and in fully differential recoil-ion momentum spectra for capture in $H_2^+ + He$ collisions [7]. In both cases the observed process did not involve any ejected electron and the interference can thus only originate from indistinguishable diffraction of the atomic (or ionic) collision partner from the two atomic centers of the molecular collision partner, as originally described by Tuan and Gerjuoy [15].

Finally, interference structures were also observed in the double differential cross sections (DDCS) for fixed projectile energy loss ε as a function of projectile scattering angle θ for target ionization in p + H_2 collisions [8]. Here, generally both types of interferences, in the ejected electron wave and in the diffracted projectile wave, can contribute. However, in that experiment the kinematic conditions were chosen such that the magnitude of the momentum transfer **q** (defined as the difference between the initial and final projectile momentum) was for most of the angular range large compared to the ejected electron momentum. Therefore, the phase angle in the interference term was not affected much by the ejected electron.

The phase angle φ in the interference resulting from the diffracted projectile wave contains two components. One component is due to the difference in the total distance that the projectile waves from the two atomic centers propagate to the detector. Only the projection of the molecular orientation onto the transverse plane (i.e. perpendicular to the initial projectile beam axis) contributes to this component of the phase angle, which we call the geometric phase angle φ_{geo}. The second component results from the change in the projectile De Broglie wavelength λ due to the ejection of the electron. The phase angle depends on where, relative to the center of mass of the molecule, the energy loss of the projectile occurs. Only the projection of the molecular orientation onto the longitudinal axis contributes to this component of the phase angle, which we call the De Broglie phase angle φ_{DB}. It should be noted that φ_{DB} is independent of θ and thus cannot by itself lead to an oscillating pattern in the angular dependence of the DDCS. Furthermore, one would expect the interference structure to not depend significantly on the ejected electron energy, which was indeed observed [8].

A switch of the symmetry between the initial and final electronic state can lead to a phase shift of π in the phase angle of the interference term [7]. Apart from such a phase jump one

would expect that the interference structure in the DDCS originating in the diffracted projectile wave is to a large extent also independent of the process occurring in the collision if the momentum of any ejected electron is small compared to q. In this article we report measurements of DDCS for ionization accompanied by fragmentation (IF) of H_2 by 75 keV proton impact, which leads to at least one positively charged fragment. Several channels contribute to IF and most of them proceed through the two-electron processes double excitation followed by auto-ionization, ionization-excitation, and double ionization [17,18]. The only one-electron process that can lead to IF is single ionization accompanied by vibrational excitation of the molecule [10,18]. The results are compared to DDCS which we measured earlier for single (non-dissociative) ionization for the same collision system [8].

Experiment

A schematic diagram of the experiment, which was performed at *Missouri S & T*, is shown in Fig. 1. A proton beam with an energy spread of much less than 1 eV was produced with a hot cathode ion source and accelerated to an energy of 75 keV. The beam was collimated by a set of slits 0.15 mm x 0.15 mm in size located 50 cm before the target region. The projectile wave packet originating from the slit has a transverse width of about 2 a.u. for this geometry, which is larger than the inter-nuclear separation of the H_2 molecule of 1.4 a.u. We recently demonstrated that an interference in the projectile wave requires a coherent projectile beam, i.e. a width of the incoming projectile wave packet that is larger than the inter-nuclear separation of the molecule. The protons were crossed with a molecular hydrogen beam produced by a supersonic jet.

The positively charged molecular fragments were extracted by an electric field of about 85 V/cm and guided onto a channel-plate detector. This relatively strong field was necessary to

efficiently collect fragments for a broad range of momenta. At this field the size of the recoil-ion detector limited the momenta of the detected fragments to about 22 a.u. (corresponding to a kinetic energy of 3.6 eV) in the plane parallel to the detector surface.

After the collision, the projectile beam was charge-analyzed by a switching magnet (not shown in Fig. 1). The protons were decelerated by 70 keV, energy-analyzed by an electrostatic parallel plate analyzer [19] and detected by a two-dimensional position-sensitive channel-plate detector. Therefore, all scattering angles θ between 0 and approximately 2 mrad were recorded simultaneously in a single run. However, the very narrow entrance and exit slits of the energy analyzer restricted recording of data to only one projectile energy loss ε at a time. The resolution in ε was ± 1.5 eV and the resolution in θ was ± 0.05 mrad. The projectile and recoil-ion detectors were set in coincidence.

Results and Discussion

In Fig. 2 a typical coincidence time spectrum is shown (recorded for $\varepsilon = 50$ eV). The time of flight of the projectile from the target region to the detector is practically constant because ε is very small compared to the initial projectile energy. Therefore, the coincidence time, i.e. the time difference between the timing of the recoil-ion and projectile signal, reflects the time of flight of the recoil-ions T_{rec}. Because T_{rec} is inversely proportional to the square root of the mass of the recoil ion, non-dissociative ionization (NDI), leading to H_2^+ ions (approx. at channel 160) is separated in the time spectrum from IF leading to proton fragments (approx. at channel 135). The DDCS for IF ($DDCS_{IF}$) could therefore be extracted by generating the projectile position spectrum with a condition on the proton peak in the time spectrum. The $DDCS_{IF}$ were normalized to the single differential cross section $d\sigma/d\varepsilon$, which, in turn, were obtained from the

ratio of the integrated proton to H_2^+ time peaks multiplied by $d\sigma/d\varepsilon$ for NDI. The latter were calculated using the semi-empirical model proposed by Rudd et al. [20], which has been very successful in reproducing measured values.

The measured $DDCS_{IF}$ are shown in Fig. 3 as a function of θ for ε = 27 (top left), 30 (top right), 40 (bottom left), and 50 eV (bottom right). The cross sections fall off rapidly with increasing θ, however, apart from this trend weak maxima can be seen for all ε at the same angle of about 1.2 mrad. At first glance the shape of the $DDCS_{IF}$ looks quite similar to what we observed earlier for NDI [8] for the same collision system. For comparison, these latter data are shown in the top panels of Fig. 4 for ε = 30 eV (left) and ε = 50 eV (right). However, a closer inspection of the $DDCS_{IF}$ reveals some differences to $DDCS_{NDI}$. An additional structure can be seen at a scattering angle around 0.6 to 0.7 mrad. This structure is not very pronounced, but it systematically occurs for all ε at the same angle and can thus not be discarded.

The structures near 0.6 to 0.7 mrad are more prominent in the ratios R between the $DDCS_{IF}$ and twice the DDCS for single ionization of atomic hydrogen ($DDCS_H$), which are plotted in Fig. 5. Experimental data for the latter [21,22] were well reproduced by a Second Born Approximation with Coulomb waves (SBA-C) at small and intermediate θ and by a continuum distorted wave – eikonal initial state (CDW-EIS) calculation at large θ [22]. We therefore combined these two calculations to obtain an essentially perfect fit to the experimental data by which we divided the measured $DDCS_{IF}$ to compute R. The same fit was also used to generate the corresponding ratios for NDI, which are shown in the bottom panels of Fig. 4 for ε = 30 eV (left) and ε = 50 eV (right)[†]. In the case of IF 3 maxima are observed in R at almost identical

[†] In the original publication of the NDI data [9] the DDCS were normalized to the CDW-EIS calculation for atomic hydrogen

angles of about 0.2, 0.7, and 1.2 mrad for all ε. In the ratios for NDI structures are seen near angles of 0.2 and 1.2 mrad as well, however, no maximum is discernable near 0.7 mrad.

In the case of NDI the interference term IT can to a good approximation be represented as the ratio between the $DDCS_{NDI}$ and the incoherent part of the cross sections $DDCS_{inc}$ [8]. Therefore, making the assumption that $DDCS_{inc}$ is twice the DDCS for atomic hydrogen, R_{NDI} is identical to IT. For a fixed molecular orientation IT is given by

$$IT = R_{NDI} = 1 + \cos(\mathbf{p_{rec}}\mathbf{D}) \quad (1)$$

where $\mathbf{p_{rec}}$ is the recoil-ion momentum vector (in the case of fragmentation it is the sum momentum of both fragments) and **D** is the position vector of one atomic center of the molecule relative to the other. If the molecular orientation is not fixed in the experiment and assuming that all orientations contribute equally the averaged interference term is [1]

$$IT = R_{NDI} = 1 + \sin(p_{rec}D)/(p_{rec}D) \quad (2)$$

However, for IF it is not as straight-forward to associate the ratios R_{IF} with the interference term because apart from the ionization of one electron it requires either a transition of the second electron or vibrational excitation of the molecule to a dissociative state. Using the approximation that this second step of IF is uncorrelated with the ionization of the first electron R_{IF} can be expressed as

$$R_{IF} = DDCS_{IF}/(2DDCS_H) = DDCS_{NDI} \times P_f/(2DDCS_H) \quad (3)$$

where P_f is the probability for the second step of IF. If we further assume that the interference term is indeed, as argued above, to a large extent independent of the specific process occurring in the collision, we obtain $R_{IF} = IT \times P_f$, where IT is the same interference term as in NDI. The differences in R between NDI and IF would then simply reflect the θ-dependence of P_f. Another possibility is that these differences are already inherent in the interference term. In that case the

observed doubling in the frequency of the interference oscillation in IF compared to NDI would suggest a much larger phase difference between the waves diffracted from the two atomic centers. Finally, it is conceivable that the interference term does not only differ in the phase angle, but its general form could be substantially altered compared to NDI. In the following we will analyze the data for specific ε in order to address these possible causes for the frequency doubling in more detail.

As mentioned above, several processes contribute to the formation of proton fragments: single ionization accompanied by vibrational dissociation (also called ground state dissociation GSD [10]), double excitation followed by autoionization (DE), ionization plus excitation (IE), and double ionization (DI). The threshold energies for these processes are (in the same order) 18, 24, 31, and 48 eV for the outer turning point of the vibrational ground state (based on potential energy curves from Sharp [23] and Guberman [24]). Thus, at ε = 27 eV only GSD and DE can contribute to the measured $DDCS_{IF}$. Experimental cross sections for these processes at the projectile energy studied here are, to the best of our knowledge, not available. However, based on DE data for p + He collisions at similar projectile energies [25,26] we have to assume that DE is quite sizeable relative to NDI in the energy-loss region where DE occurs. On the other hand, only some doubly excited states are accessible at ε =27 eV and this energy loss is only 3 eV above the threshold for the lowest lying state ($^1\Sigma_g^+$). Furthermore, even this state can only be populated near the outer turning point. The Franck-Condon regime for transitions from the electronic and vibrational ground state covers internuclear distances from about D = 1.2 a.u. to 1.7 a.u., but at ε = 27 eV DE is energetically possible only for D > 1.5 a.u.. Finally, for GSD kinetic energy releases (KER) per fragment of more than 1 eV are entirely negligible [18] so that for this process all proton fragments are guided onto the recoil-ion detector. In contrast, for DE

the KER spectrum at $\varepsilon = 27$ eV extends out to energies of about 4.5 eV per fragment so that here not all fragmentation events are detected. Therefore, the fraction of the $DDCS_{IF}$ due to GSD could be important as well. The total cross section ratio between GSD and NDI for fast proton impact is expected to be approximately 1.5% independent of the projectile velocity [27]. Our measured ratio between the single differential cross sections $d\sigma/d\varepsilon$ for IF and NDI is about 2.2%. We therefore crudely estimate that GSD contributes about 2/3 and DE 1/3 of the $DDCS_{IF}$ at ε =27 eV.

At $\varepsilon = 30$ eV, GSD and DE seem to contribute approximately equally to fragmentation. At ε = 40 eV DE is energetically no longer accessible in the Franck-Condon region for most doubly excited states. Therefore, at this energy loss only GSD and IE contribute to formation of proton fragments. Finally, $\varepsilon = 50$ eV is just barely above the threshold for DI so that here, too, IF is dominated by GSD and IE. Furthermore, it should be noted that for IE the KER/fragment spectrum covers a range between 3 eV and 13 eV and for DI between 7 eV and 14 eV [18]. Therefore, most fragments produced by IE and all fragments produced by DI will not be detected if the molecule is oriented in the plane of the recoil-ion detector surface because of the limited momentum acceptance mentioned above.

In Fig. 6 we present $P_f = DDCS_{IF}/DDCS_{NDI}$ as a function of scattering angle for $\varepsilon = 27$ eV. These ratios exhibit essentially the same oscillatory pattern as R_{IF}. We therefore do not believe that the differences in R between IF and NDI can be explained by the θ-dependence of P_f, at least not under the assumption that IF can be viewed as a combination of two (or more) independent processes.

Next, we consider the possibility that the doubling of the interference frequency may be caused by a larger phase angle in IF compared to NDI. As mentioned above, for NDI and for a

fixed molecular orientation the phase angle is given by $\varphi = \mathbf{p}_{rec}\ \mathbf{D}$. For our kinematics the electron momentum is small compared to q for most scattering angles so that to a good approximation $\varphi = q\ D \cos\alpha$, where α is the angle enclosed by **q** and **D**. Therefore, φ and thereby the oscillation frequency maximize when the molecule is aligned along the momentum transfer vector and for D = 1.7 a.u., which is the largest inter-nuclear separation within the Franck-Condon region. It should be noted that GSD actually is more likely to take place near the inner turning point. But even for this maximized φ the oscillation frequency of the interference term is about a factor of 2 smaller than what we observe in the experiment.

The inability of equation (1) to reproduce the doubling of the interference frequency observed for GSD compared to NDI even under most favorable assumptions raises the question whether this form of IT is valid for GSD. Strong indications that this may not be the case were reported by Senftleben et al. [10], who measured fully differential cross sections (FDCS) for fixed molecular orientation for the same process for electron impact. For kinematic conditions which roughly correspond to $\theta \approx 0.7$ mrad in our data they observed constructive interference if the molecule was oriented parallel to **q** and destructive interference if it was oriented perpendicular to **q**. In contrast, the IT based on equation (1) predicts destructive interference for the parallel orientation and constructive interference for the perpendicular orientation. On the other hand, the molecular 3-body distorted wave (M3DW) approach [28], which is not based on equation (1), qualitatively reproduced the data of Senftleben et al. These observations correspond with the behavior of our $DDCS_{IF}$ data around 0.6 to 0.7 mrad: here, too, we observe constructive interference while in corresponding data for NDI, which were found to be consistent with equation (1), destructive interference was observed in the same angular range [8]. The

conclusion of Senftleben et al. that the interference of equation (1) is not applicable to GSD is thus not inconsistent with the present data.

The observation that R_{IF} hardly differs at all for the larger energy losses from ε = 27 eV suggests that if equation (1) indeed does not hold for GSD this may also be true for proton fragment production through DE, IE, or DI. For ε = 30 eV, although DE is likely an important channel, we cannot entirely rule out that IF is dominated by GSD. However, a closer inspection of the coincidence time spectra leaves no doubt that for ε = 40 and 50 eV at least IE plays an important role. In Fig. 7 the proton time peak is expanded and plotted in higher resolution than in Fig. 2, which shows the time spectrum compressed by a factor of 4. The dashed and solid curves represent the time spectra for ε = 30 and 50 eV, respectively. These plots reveal that for ε = 50 eV the fragmentation leads to a triple peak, but at ε = 30 eV we only observe a single peak. The spectra for ε = 27 and 40 eV are practically identical to those for ε = 30 and 50 eV, respectively. The side peaks at the larger energy losses represent fragments which are ejected with large momentum towards (left peak) or away from (right peak) the recoil-ion detector. Since for GSD KER values larger than approximately 1 eV are entirely negligible and DE is no longer accessible for most states at energy losses of 40 eV and above these contributions must come from IE. At ε =50 eV a small fraction from DI may also be present.

The center peak contains two components, one from GSD and one from IE and DI leading to fragments with small momenta in the direction of the extraction field (i.e. perpendicular to the plane of the detector). Since the KER spectra for these latter two processes only start at about 3 eV/fragment and the average energy is about 7 eV for IE and 9.5 eV for DI such events only contribute to the center peak if the molecule was oriented at some minimal angle relative to the extraction field. However, that angle cannot be too large either because otherwise the fragments

would not be detected due to the limited momentum acceptance of the detector. One would therefore expect such events to contribute to the regions in between the center and side peaks. The fact that these structures are separated from each other by minima suggests that the center peak is dominated by GSD. This is also supported by the observation that the ratio between the time peak contents for the slow p fragments and the H_2^+ ions of about 1.3% is very close to the expected ratio between the total cross sections for GSD and NDI (see above).

In the top panels of Fig. 8 we show the $DDCS_{IF}$ with an additional condition on the time peak for the slow fragments (closed symbols) and for the fast fragments (open symbols) for ε = 40 eV (left panel) and for ε = 50 eV (right panel). The data for the fast fragments should be viewed as triple differential cross sections TDCS = $d^3\sigma/(d\Omega_p d\varepsilon d\Omega_m)$ for IE (and possibly a small component of DI for ε = 50 eV, which we neglect in the following) because the molecular orientation is now determined. However, the TDCS are not properly normalized since we do not know the effective solid angle for the detection of the molecular fragments. In contrast, the data for the slow fragments still represent DDCS for GSD (neglecting possible contributions from IE and DI) since they contain all molecular orientations due to the very small KER resulting from this process.

The TDCS for IE look very similar to the $DDCS_{IF}$ without the condition on the proton time peak for both energy losses. The ratios between these TDCS and twice the $DDCS_H$, plotted in the bottom panels of Fig. 8, show that the interference structure still exhibits a doubling of the oscillation frequency compared to the data for NDI. In contrast, the interference structure in the $DDCS_{IF}$ for GSD is strongly suppressed. Only the first maximum around 0.2 mrad is still visible in the ratios (at least at ε = 50 eV). But the two maxima at the larger scattering angles are completely absent, except, perhaps, for a trace of a maximum near 0.7 mrad for ε = 50 eV.

Therefore, while for IE we find a similar behavior as for NDI in so far as the structures in the θ-dependence of the cross sections do not depend very sensitively on the energy loss, the data for GSD are much more affected by ε.

A strong suppression of the interference structure at large ε we also observed for NDI [8]. However, there this effect only occurred around energy losses corresponding to ejected electron speeds v_{el} equal to the projectile speed v_p (i.e. for ε ≈ 56 eV). In that work we therefore considered the possibility that the suppression of the interference structure may be correlated with the post-collision interaction (PCI) between the outgoing projectile and the ejected electron, which is known to maximize at the matching velocity $v_{el} = v_p$ [29,30]. Such a correlation is not confirmed by the present data for GSD because the interference structures are essentially absent already at ε = 40 eV, while the matching velocity corresponds to ε = 59 eV. A possible alternative explanation is based on the molecular orientation. If the molecule was always oriented along the projectile beam axis the phase angle φ would not depend on θ. For NDI we found that the molecular orientation itself depended on θ favoring longitudinal (i.e. parallel to the projectile beam) orientations at large θ and transverse orientations at intermediate θ. If the orientation remained fixed along the longitudinal direction over an extended range of scattering angles, no interference oscillation would be present in that range, while such structure could still occur at other θ. We therefore consider the possibility that GSD favors longitudinal molecular orientations over a much larger angular range than in NDI, possibly down to scattering angles as small as approximately 0.5 mrad (or smaller). One could then understand why the peak structures at 0.7 and 1.2 mrad, observed for ε = 27 and 30 eV, essentially disappear at larger ε, but that the maximum near 0.2 mrad nevertheless survives. However, at present we cannot offer an explanation why GSD would favor longitudinal orientations more than NDI does.

An alternative explanation for the doubling of the oscillation frequency emerges if causes for the structures other than molecular interference are considered. In the differential cross sections for DE in p + He collisions, as well as in the ratio to differential single excitation cross sections, a maximum was observed at around 0.7 mrad [25,26], i.e. at roughly the same angle where the second oscillation maximum occurs in the present data. Similar structures were also observed in corresponding ratios for other two-electron processes, like e.g. DI [31], transfer ionization [32,33], or double capture [34] at about the same angle (except for DI). They were interpreted as due to interference between first- and higher-order transition amplitudes. For DE these structures were not observed for projectile energies below 150 keV. However, it should be noted that for H_2 the excitation energy is about a factor of 2 smaller than for He. Therefore the projectile energy relative to the excitation energy in the present case is comparable to the DE studies for p + He collisions. It is reasonable to assume that such structures exist for IE as well, although these ratios have not been measured yet for this process. The oscillations in the present data could then be explained by a combination of two independent components: 1.) interference due to diffraction from the two atomic centers of the molecule, leading to the maxima near 0.2 and 1.2 mrad, and 2.) interference between first- and higher-order transition amplitudes leading to the maxima around 0.7 mrad.

Conclusions

We have measured double differential cross sections (DDCS) for fragmentation of H_2 leading to at least one proton by 75 keV p impact for fixed energy losses ε as a function of scattering angle θ. In the θ-dependence we observed an oscillating pattern for all ε. Several processes contribute to proton fragment formation. Ionization accompanied by vibrational dissociation and/or double

excitation are the dominant channels at small ε and ionization plus excitation at large ε. Nevertheless, the data for different ε are very similar to each other, but, surprisingly, the frequency of the oscillation is about twice as large as what was observed for non-dissociative ionization (NDI) for the same collision system [8].

At this time we cannot conclusively trace the origin of the frequency doubling compared to NDI. However, two possible alternative explanations emerge from the data analysis: first, the interference term which qualitatively describes various data sets for NDI [e.g. 1-6,8] may not be applicable if ionization is accompanied by fragmentation of the molecule. Indications that this may be the case were reported earlier [10]. Second, the oscillation may be due to a combination of interference between the projectile waves diffracted at the two atomic centers of the molecule and interference between first- and higher-order amplitudes for the involved two-electron processes. We are currently preparing experiments, in which the kinetic energy release in the fragmentation will be measured. It will then be possible to isolate ionization accompanied by vibrational dissociation from the two-electron processes. A persistence of the frequency doubling would indicate that the interference term for fragmentation process indeed has a different form than for NDI. On the other hand, a frequency similar to what is observed for NDI would suggest that the frequency doubling is characteristic to two-electron processes. Interference between first- and higher order scattering amplitudes would then represent a plausible explanation.

Acknowledgements

Support by the National Science Foundation under grant no. PHY-0969299 is gratefully acknowledged.

Reference

[1] N. Stolterfoht, B. Sulik, V. Hoffmann, B. Skogvall, J. Y. Chesnel, J. Ragnama, F. Frèmont, D. Hennecart, A. Cassimi, X. Husson, A. L. Landers, J. Tanis, M. E. Galassi, and R. D. Rivarola, Phys. Rev. Lett. **87** 23201 (2001).

[2] N. Stolterfoht et al., Phys. Rev. A **67**, 030702 (2003)

[3] D. Misra, U. Kadhane, Y. P. Singh, L. C. Tribedi, P. D. Fainstein, and P. Richard Phys. Rev. Lett. **92**, 153201 (2004)

[4] D. S. Milne-Brownlie, M. Foster, Junfang Gao, B. Lohmann, and D. H. Madison, Phys. Rev. Lett. **96**, 233201 (2006)

[5] D. Misra, A. Kelkar, U. Kadhane, Ajay Kumar, Lokesh C. Tribedi, and P. D. Fainstein Phys. Rev. A **74**, 060701 (2006)

[6] E.M. Staicu Casagrande, A. Naja, F. Mezdari, A. Lahmam-Bennani, P. Bolognesi, B. Joulakian, O. Chuluunbaatar, O. Al-Hagan, D. H. Madison, D.V. Fursa and I. Bray, J. Phys. B **41**, 025204 (2008)

[7] L. Ph. H. Schmidt, S. Schössler, F. Afaneh, M. Schöffler, K. E. Stiebing, H. Schmidt-Böcking, and R. Dörner, Phys. Rev. Lett. **101**, 173202 (2008)

[8] J.S. Alexander, A.C. Laforge, A. Hasan, Z.S. Machavariani, M.F. Ciappina, R.D. Rivarola, D.H. Madison, and M. Schulz, Phys. Rev. **A78**, 060701(R) (2008)

[9] D. Misra, H.T. Schmidt, M. Gudmundsson, D. Fischer, N. Haag, H.A.B. Johansson, A. Källberg, B. Najjari, P. Reinhed, R. Schuch, M. Schöffler, A. Simonsson, A.B. Voitkiv, and H. Cederquist, Phys. Rev. Lett. **102**, 153201 (2009)

[10] A. Senftleben, T. Pflüger, X. Ren, O. Al-Hagan, B. Najjari, D.H. Madison, A. Dorn, J. Ullrich, J. Phys. B **43**, 081002 (2010)

[11] C. R. Stia, O. A. Fojón, P. F. Weck, J. Hanssen, B. Joulakian, and R. D. Rivarola Phys. Rev. A **66**, 052709 (2002)

[12] M. E. Galassi, R. D. Rivarola, and P. D. Fainstein, Phys. Rev. A **70**, 032721 (2004)

[13] M. F. Ciappina and R. D. Rivarola, J. Phys. B **41** 015203 (2008)

[14] J. Colgan, O. Al-Hagan, D.H. Madison, C. Kaiser, A.J. Murray, M.S. Pindzola, Phys. Rev. A **79**, 052704 (2009)

[15] T. F. Tuan and E. Gerjuoy, Phys. Rev. **117**, 756 (1960)

[16] S. Cheng, C. L. Cocke, V. Frohne, E. Y. Kamber, J. H. McGuire, and Y. Wang, Phys. Rev. A **47**, 3923 (1993)

[17] A. K. Edwards, R. M. Wood, A. S. Beard, and R. L. Ezell, Phys. Rev. A **37**, 3697 (1988)

[18] A. K. Edwards, R. M. Wood, J.L. Davis, and R. L. Ezell, Phys. Rev. A **42**, 1367 (1990)

[19] A.D. Gaus, W. T. Htwe, J. A. Brand, T. J. Gay, and M. Schulz, Rev. Sci. Instrum. **65** 3739 (1994)

[20] M.E. Rudd, Y.-K. Kim, D.H. Madison, and T.J. Gay, Rev. Mod. Phys. **64**, 441 (1992)

[21] A.C. Laforge, K.N. Egodapitiya, J.S. Alexander, A. Hasan, M.F. Ciappina, M.A. Khakoo, and M. Schulz, Phys. Rev. Lett. **103**, 053201 (2009)

[22] M. Schulz, A.C. Laforge, K.N. Egodapitiya, J.S. Alexander, A. Hasan, M.F. Ciappina, A.C. Roy, R. Dey, A. Samolov, and A.L. Godunov, Phys. Rev. A **81**, 052705 (2010)

[23] T.E. Sharp, At. Data **2**, 119 (1971)

[24] S.L. Guberman, J. Chem. Phys. **78**, 1404 (1983)

[25] W.T. Htwe, T. Vajnai, M. Barnhart, A.D. Gaus, and M. Schulz, Phys. Rev. Lett. **73**, 1348 (1994)

[26] M. Schulz, W.T. Htwe, A.D. Gaus, J.L. Peacher, and T. Vajnai, Phys. Rev. A **51**, 2140 (1995)

[27] I. Ben-Itzhak, V. Krishnamurthi, K.D. Carney, H. Aliabadi, H. Knudsen, U. Mikkelsen, and B.D. Esry, J. Phys. B **29**, L21 (1996)

[28] J. Gao, J. L. Peacher, and D. H. Madison, J. Chem. Phys. **123**, 204302 (2005)

[29] T. Vajnai, A.D. Gaus, J.A. Brand, W. Htwe, D.H. Madison, R.E. Olson, J.L. Peacher, and M. Schulz, Phys. Rev. Lett. **74**, 3588 (1995)

[30] M. Schulz, T. Vajnai, A.D. Gaus, W. Htwe, D.H. Madison, and R.E. Olson, Phys. Rev. A **54**, 2951 (1996)

[31] J. P. Giese and E. Horsdal, Phys. Rev. Lett. **60**, 2018 (1988)

[32] E. Horsdal, B. Jensen, and K. O. Nielsen, Phys. Rev. Lett. **57**, 1414 (1986)

[33] S.W. Bross, S.M. Bonham, A.D. Gaus, J.L. Peacher, T. Vajnai, H. Schmidt-Böcking, and M. Schulz, Phys. Rev. A **50**, 337 (1994)

[34] M. Schulz, T. Vajnai, and J.A. Brand, Phys. Rev. A **75**, 022717 (2007)

Figure Captions

Fig. 1: Schematic diagram of the experimental set-up.

Fig. 2: Projectile – recoil ion coincidence time spectrum. The peak structures near channels 135 and 160 represent proton fragment and H_2^+ formation, respectively.

Fig. 3: Double differential cross sections (DDCS) for proton fragment formation plotted as a function of the projectile scattering angle θ for fixed energy losses ε of 27 (top left), 30 (top right), 40 (bottom left), and 50 eV (bottom right), respectively.

Fig. 4: DDCS for non-dissociative ionization (NDI) are plotted in the top panels as a function of the projectile scattering angle θ for fixed energy losses ε of 30 and 50 eV, respectively. The bottom panels show the ratios between the DDCS for NDI and twice the DDCS for single ionization of atomic hydrogen for the same energy losses.

Fig. 5: Ratios between the measured DDCS for proton fragment formation of Fig. 3 and twice the DDCS for atomic hydrogen as a function of scattering angle for the same energy losses as in Fig. 3.

Fig. 6: Ratios P_f between the measured DDCS for proton fragment and H_2^+ formation as a function of scattering angle for ε = 27 eV.

Fig. 7: Projectile – recoil ion coincidence time spectrum for ε = 30 eV (dashed curve) and ε = 50 eV (solid curve) expanded over the region of the proton fragment peak. The resolution is improved compared to the time spectrum of Fig. 2 because the latter is compressed by a factor of 4.

Fig. 8: DDCS for proton fragment formation are plotted in the top panels as a function of the projectile scattering angle θ for fixed energy losses ε of 40 and 50 eV, respectively, with additional conditions on the time peak labeled “slow fragments” (closed symbols) and “fast fragments” (open symbols) in Fig. 7. The bottom panels show the corresponding ratios between these DDCS and twice the DDCS for single ionization of atomic hydrogen.

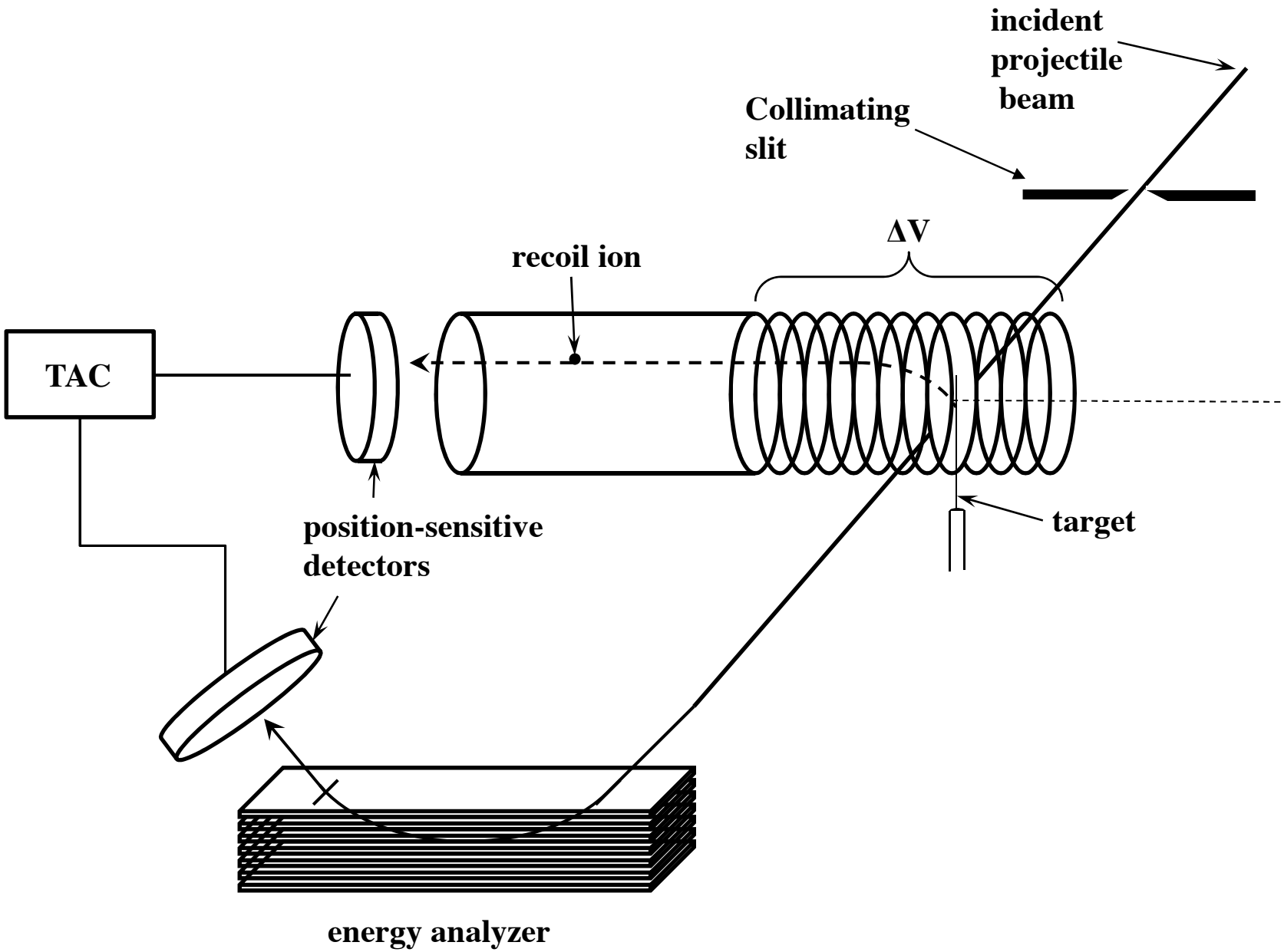
incident
projectile
beam
Collimating
slit
ΔV
recoil ion
TAC
position-sensitive
detectors
target
energy analyzer

Fig. 1

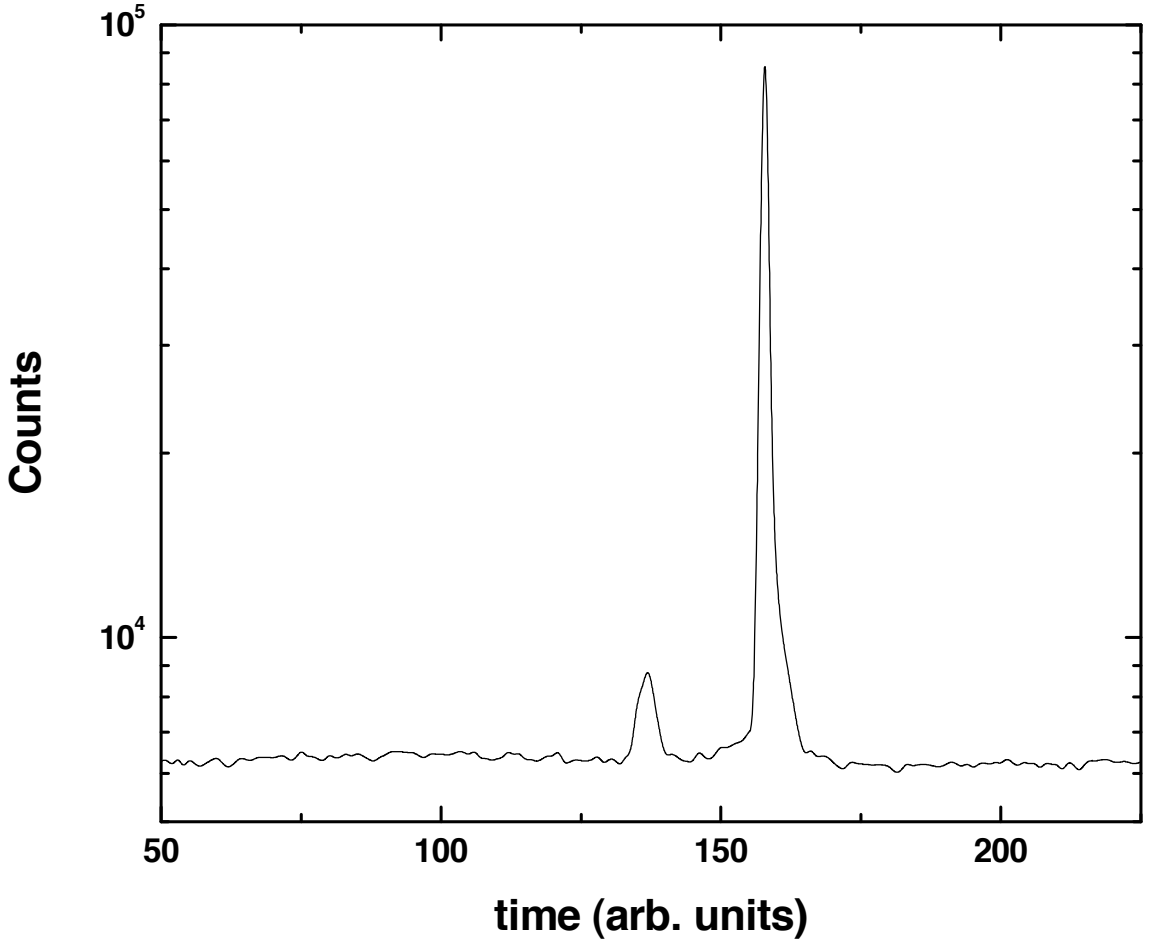

Fig. 2

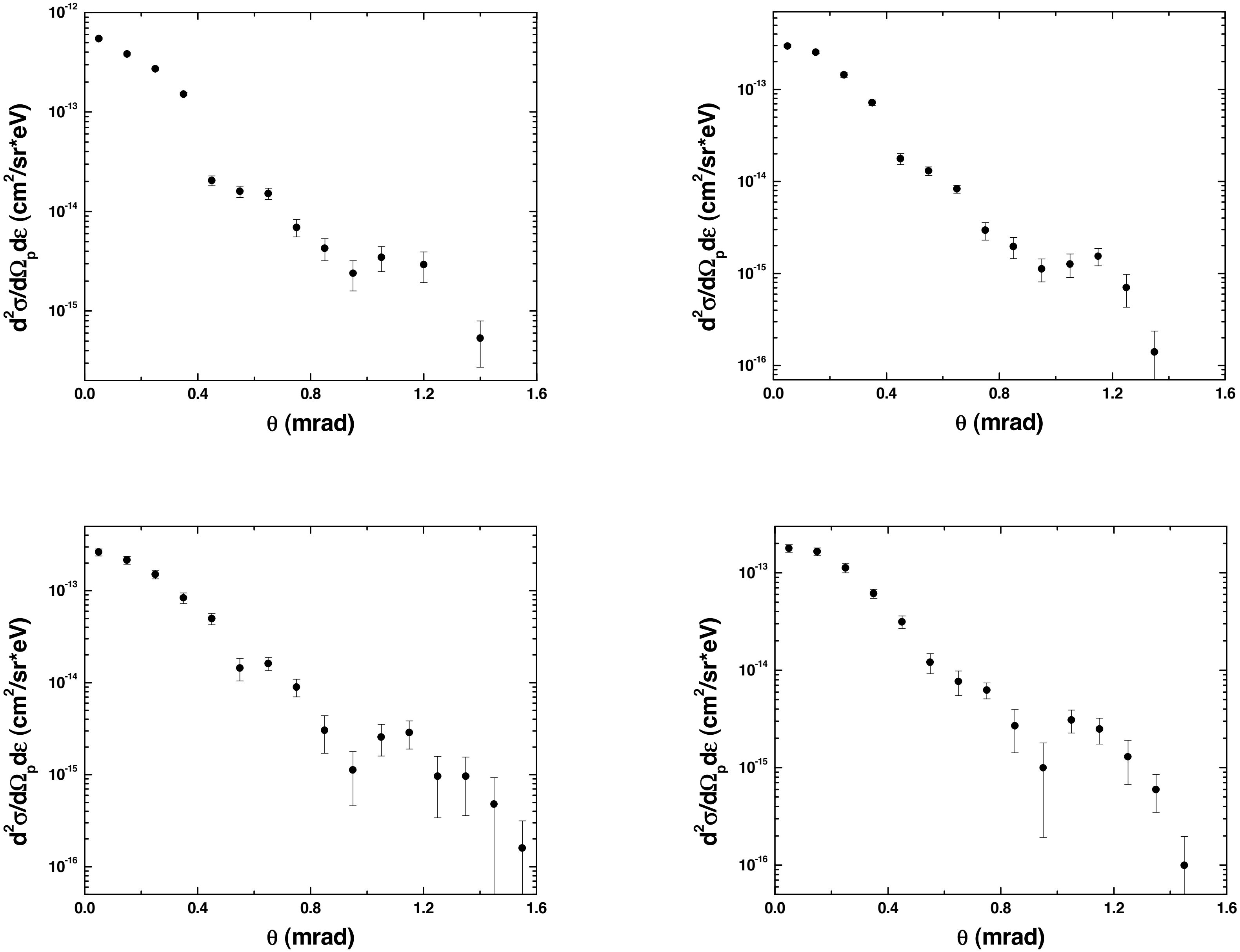

Fig. 3

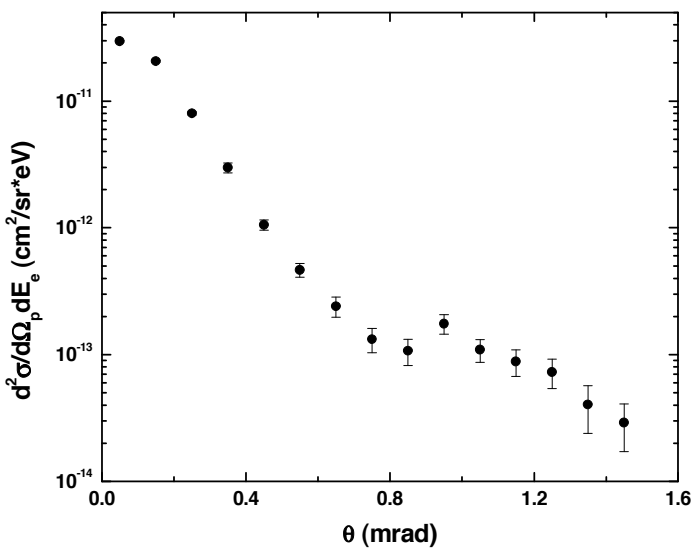
$d^2\sigma/d\Omega_p dE_e$ (cm^2/sr*eV)
10^{-11}
10^{-12}
10^{-13}
10^{-14}
0.0
0.4
0.8
1.2
1.6
θ (mrad)

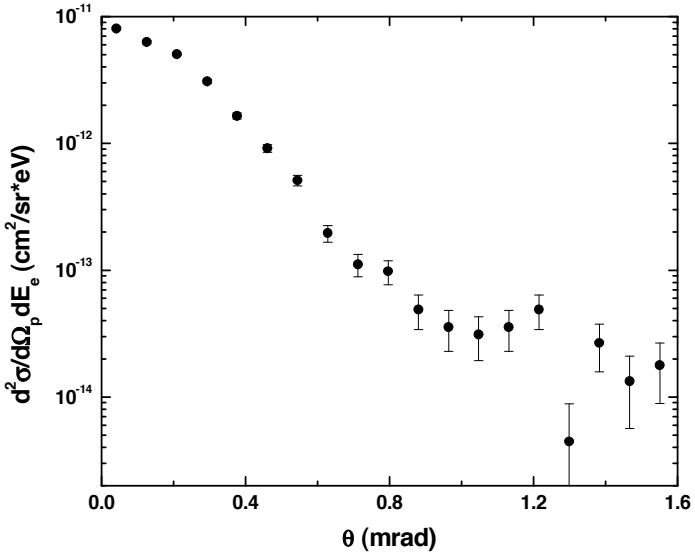
$d^2\sigma/d\Omega_p dE_e$ (cm^2/sr*eV)
10^{-11}
10^{-12}
10^{-13}
10^{-14}
0.0
0.4
0.8
1.2
1.6
θ (mrad)

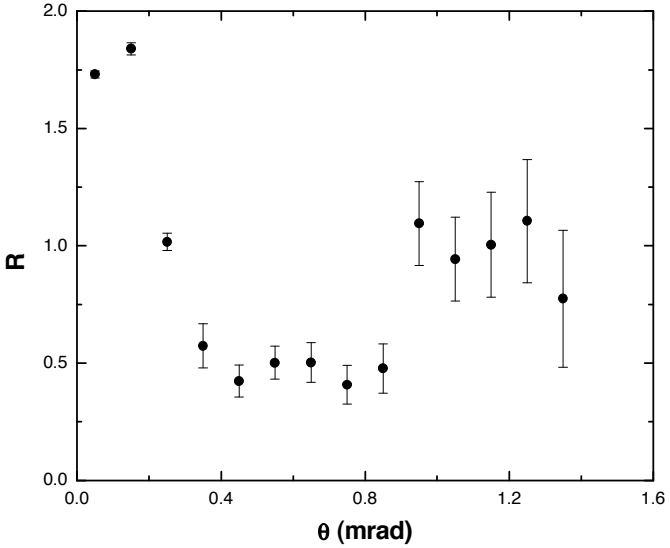
R
2.0
1.5
1.0
0.5
0.0
0.0
0.4
0.8
1.2
1.6
θ (mrad)

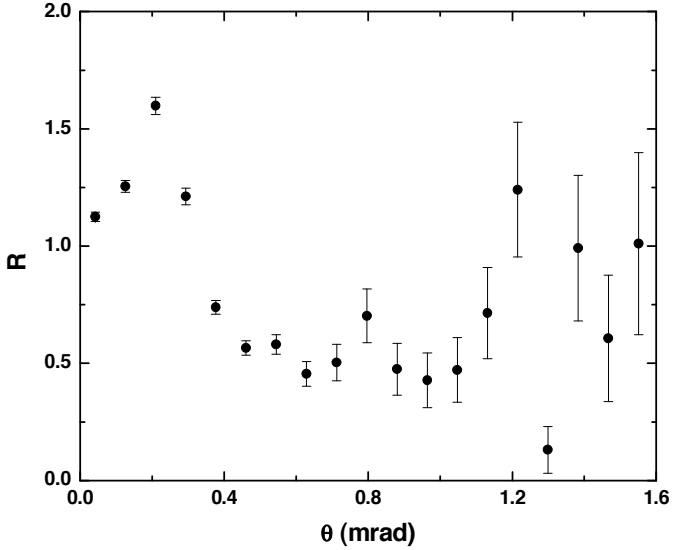
R
2.0
1.5
1.0
0.5
0.0
0.0
0.4
0.8
1.2
1.6
θ (mrad)

Fig. 4

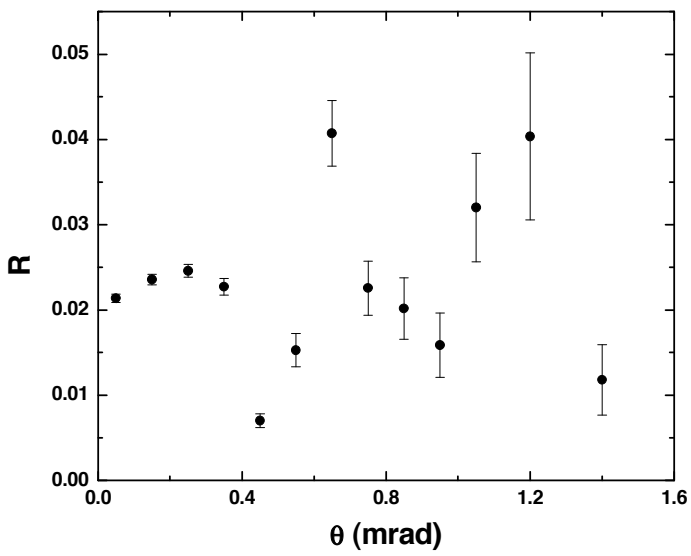
R
θ (mrad)
0.00
0.01
0.02
0.03
0.04
0.05
0.0
0.4
0.8
1.2
1.6

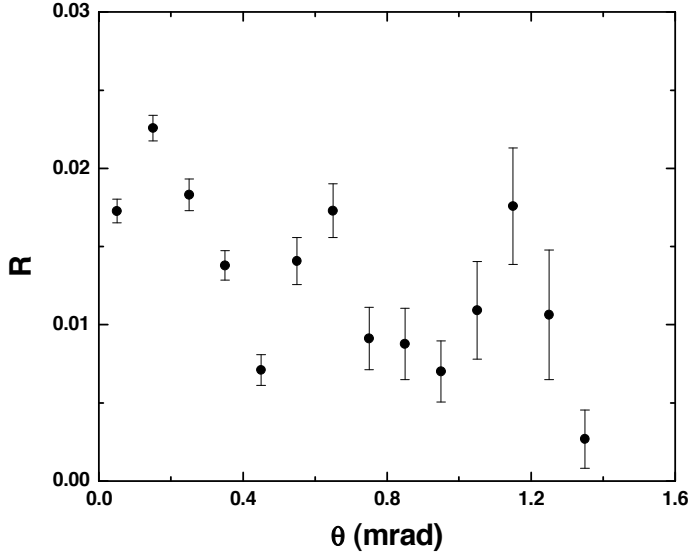
R
θ (mrad)
0.00
0.01
0.02
0.03
0.0
0.4
0.8
1.2
1.6

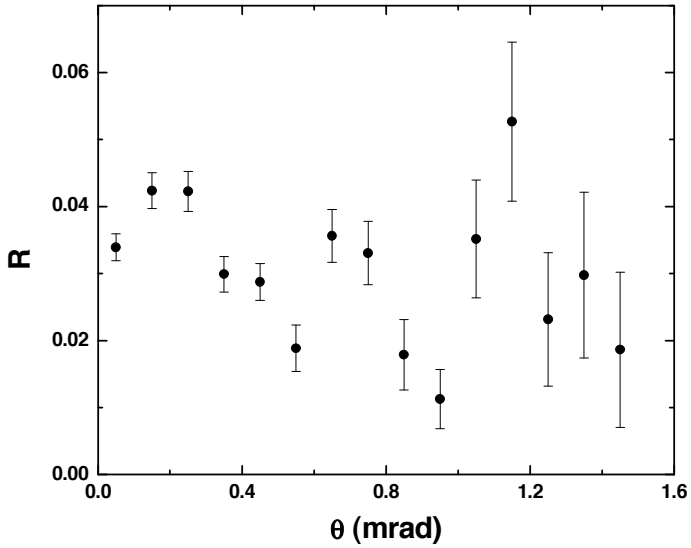
R
θ (mrad)
0.00
0.02
0.04
0.06
0.0
0.4
0.8
1.2
1.6

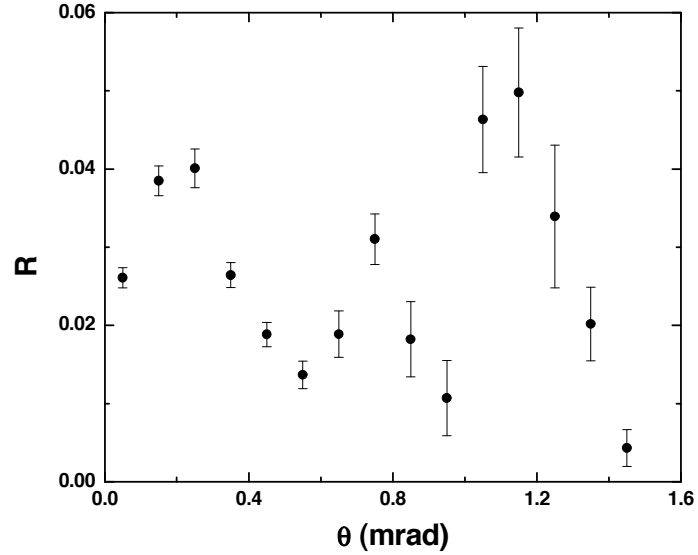
R
θ (mrad)
0.00
0.02
0.04
0.06
0.0
0.4
0.8
1.2
1.6

Fig. 5

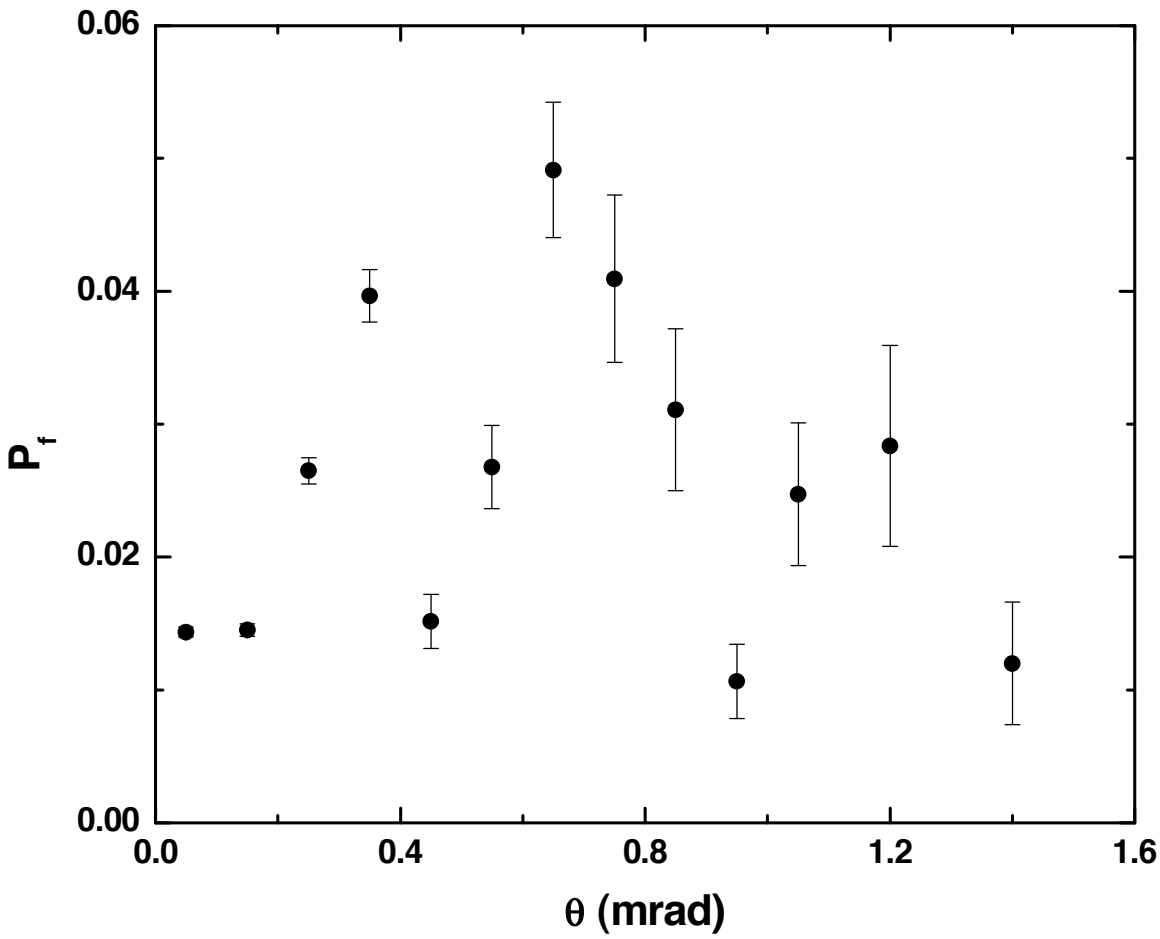

Fig. 6

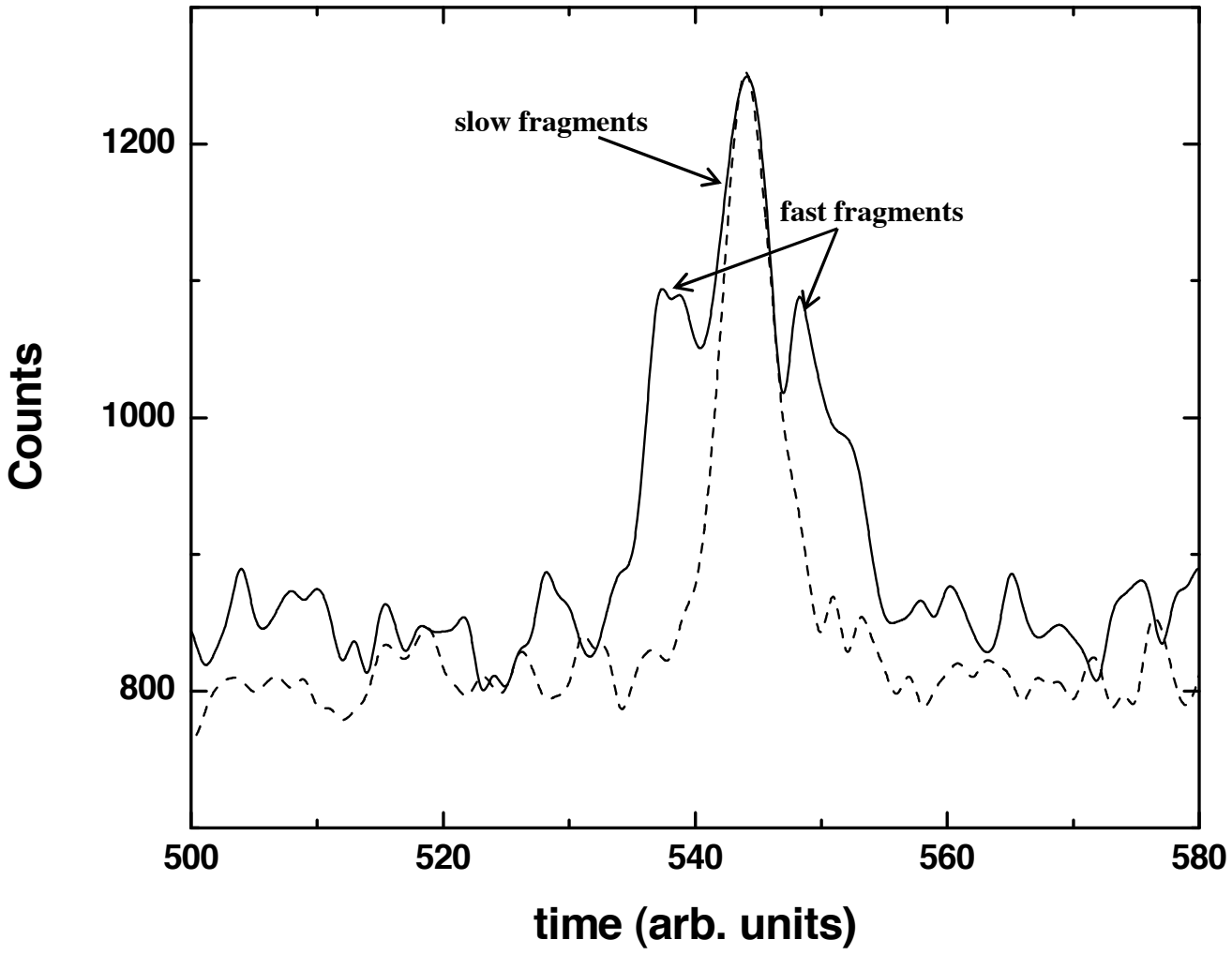
slow fragments
fast fragments
Counts
1200
1000
800
500
520
540
560
580
time (arb. units)

Fig. 7

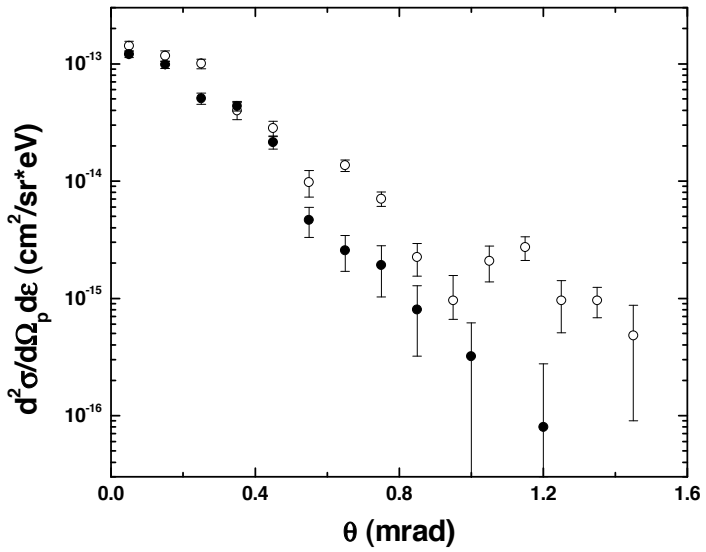
10^{-13}
10^{-14}
10^{-15}
10^{-16}
$d^2\sigma/d\Omega_p d\varepsilon$ (cm^2/sr*eV)
0.0
0.4
0.8
1.2
1.6
θ (mrad)

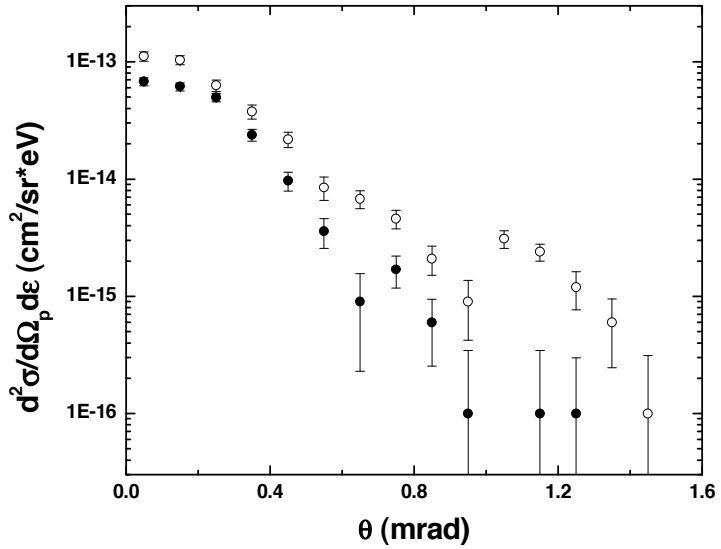
1E-13
1E-14
1E-15
1E-16
$d^2\sigma/d\Omega_p d\varepsilon$ (cm^2/sr*eV)
0.0
0.4
0.8
1.2
1.6
θ (mrad)

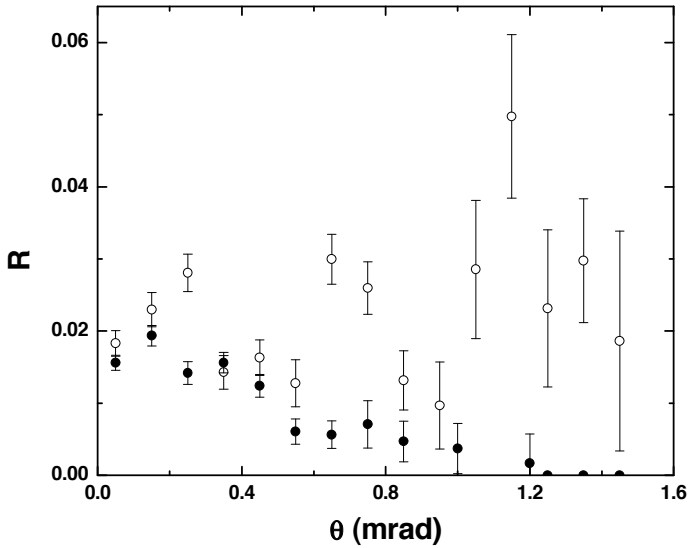
R
0.06
0.04
0.02
0.00
0.0
0.4
0.8
1.2
1.6
θ (mrad)

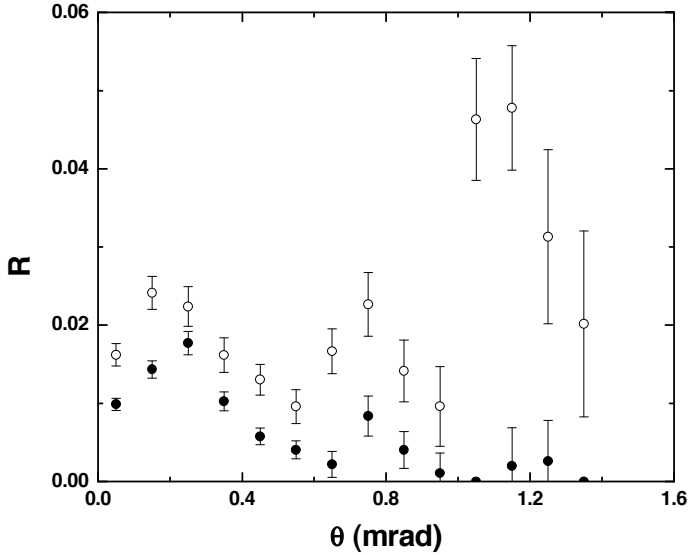
R
0.06
0.04
0.02
0.00
0.0
0.4
0.8
1.2
1.6
θ (mrad)

Fig. 8